Heliyon 9 (2023) e18082

Contents lists available at ScienceDirect

Heliyon

journal homepage: www.cell.com/heliyon

Loss of Flot2 expression in deep cerebellar nuclei neurons of mice with Niemann-Pick disease type C

Tsu-I Chen [a,1], Pei-Chun Hsu [b,1], Ni-Chung Lee [a,b], Yu-Han Liu [a], Hao-Chun Wang [b], Yen-Hsu Lu [a], Yin-Hsiu Chien [a,b], Wuh-Liang Hwu [a,b,c,*]

[a] Department of Pediatrics, National Taiwan University Hospital and National Taiwan University College of Medicine, Taipei, Taiwan
[b] Department of Medical Genetics, National Taiwan University Hospital, Taipei, Taiwan
[c] Graduate Institute of Integrated Medicine, China Medical University, Taichung City, Taiwan

ARTICLE INFO

Keywords:
Niemann-Pick disease type C
Deep cerebellar nuclei
GM2 ganglioside
Flot2
Lipid rafts
N-acetyl L-leucine

ABSTRACT

Niemann-Pick disease type C (NPC) is caused by a deficiency of the *NPC1* or *NPC2* gene, leading to storages of unesterified cholesterol and sphingolipids. Cerebellar ataxia is a main symptom of NPC and the deep cerebellar nuclei (DCN) is the sole signal output of the cerebellum. In this study, we explored the pathological changes in DCN neurons of *Npc1* knockout mice (*Npc1*$^{-}$). We first demonstrated that DCN neurons of *Npc1*$^{-}$ mice had prominent ganglioside GM2 accumulation in the late endosomes but not in the lysosomes. More importantly, Flot2 expression, a marker for the lipid rafts, was lost. Single-nucleus RNA sequencing analysis revealed a generalized reduction in gene expression in DCN neurons, though *Camk1d*, encoding one of the Ca^{2+}/calmodulin-dependent protein kinases (CaMKs), increased in expression. We treated *Npc1*$^{-}$ mice with CaMK inhibitor KN-93, but CaMK1D expression increased further. We also fed *Npc1*$^{-}$ mice with two medications for NPC. We found that miglustat, a sphingolipid synthesis inhibitor, increased the expression of Flot2. Moreover, N-acetyl L-leucine (NALL), an experimental medicine for NPC, recovered Flot2 expression. Therefore, our data suggest that in *Npc1*$^{-}$ mice, GM2 sequestration and the loss of lipid rafts lead to cell dysfunction and symptoms of NPC.

1. Introduction

Niemann-Pick disease type C (NPC) is a disorder (OMIM number 257220) caused by autosomal recessive inheritance of mutations in either of two genes, *NPC1* (in approximately 95% of cases) or *NPC2* (in approximately 4% of cases) [1–3]. The NPC1 protein is located on vesicles that contain LAMP1, lysosomes, or on vesicles that do not contain LAMP1, endosomes [4]. NPC is characterized by abnormalities in intracellular transport of endocytosed cholesterol with sequestration of unesterified cholesterol in lysosomes and late endosomes [5]. Incubation of fibroblasts with low-density lipoprotein increased colocalization of NPC1 within LAMP1-containing compartments [4], and filipin staining of the treated fibroblasts has become a standard method for the diagnosis of NPC [6]. Cholesterol and sphingolipids also accumulated in Rab7-positive late endosomes in cultured cells from *Npc1*$^{-}$ mice [7]. There are several possible explanations for the sphingolipid accumulation in NPC. First, altered vesicular transport may lead to storage, as shown by Annexin 2, a membrane-associated protein that joins endocytic trafficking to the Golgi apparatus, being diverted to the late

* Corresponding author. Department of Pediatrics, National Taiwan University Hospital 8 Chung-Shan South Road, Taipei 10041, Taiwan.
E-mail address: hwuwlntu@ntu.edu.tw (W.-L. Hwu).
[1] The first two authors contributed equally.

https://doi.org/10.1016/j.heliyon.2023.e18082
Received 5 September 2022; Received in revised form 13 May 2023; Accepted 6 July 2023
Available online 7 July 2023

endosomes in NPC [8]. Second, cholesterol is a potent inhibitor of sphingolipid activator proteins [9]. Additionally, sphingosine storage can cause altered calcium homeostasis, leading to the secondary storage of sphingolipids and cholesterol [10].

In the liver and spleen of patients with NPC, accumulated lipids include unesterified cholesterol, glycolipids, and free sphingosine. In the brain, neither cholesterol nor sphingomyelin overtly accumulates, but there is significant accumulation of glucosylceramide, lactosylceramide, gangliosides GM2, and GM3 [8,10]. The clinical presentations of NPC are highly heterogeneous. Systemic symptoms, including neonatal jaundice and hepatosplenomegaly, usually occur early in the course of disease [11]. Characteristic neurological signs include vertical supranuclear gaze palsy, gelastic cataplexy, and cerebellar signs (ataxia, dystonia/dysmetria, dysarthria, and dysphagia) [5]. Miglustat, a drug that decreases the synthesis of sphingolipids, stabilizes the neurological and swallowing functions in patients with NPC [12,13]. Intrathecal 2-hydroxypropyl-beta-cyclodextrin, a compound known to bind cholesterol, also slows disease progression [14]. Recently, N-acetyl L-leucine (NALL) was also shown to slows the disease progression in patients with NPC [15,16].

Purkinje cells of *Npc1*$^{-}$ mice show GM2 accumulation and subsequently die [17,18]. Although Purkinje cells are relatively preserved in patients with NPC [19], cerebellar ataxia is still a prominent symptom. Purkinje cells elaborate extensive dendrites into the molecular layer and receive input from a large number of parallel fibers and climbing fibers. Purkinje cells send GABAergic projects to the deep cerebellar nuclei (DCN), clusters of gray matter lying within the white matter at the core of the cerebellum, which are the only output of the cerebellar cortex. Neurons in the DCN can be classified by morphological, electrophysiological, and biochemical properties into glutamatergic projection neurons, GABAergic and glycinergic projection neurons, and GABAergic, glycinergic, and glutamatergic interneurons [20]. We hypothesized that DCN dysfunction may contribute to the cerebellar symptoms of NPC. In the current study, we explore the pathological changes in DCN neurons of *Npc1*$^{-}$ mice. We found that, by staining of the lipid raft scaffold protein Flotillin-2 (Flot2) [21], lipid rafts were lost in these neurons. The two current treatments for NPC, Miglustat and NALL, both improved the expression of Flot2.

2. Materials and methods

2.1. Animals

Npc1^{-} mice (*Npc1*^{m1N}, Jax stock, #003092) were created by using 824 bp retrotransposon-like DNA to replace 703 bp of the wild-type genomic sequence spanning 44 bp of an exon [17]. These mice, in our animal facility, developed symptoms at approximately 7 weeks of age and reached the humane endpoint at ages 9–10 weeks. The experimental procedures were approved by the National Taiwan University College of Medicine and the College of Public Health Institutional Animal Care and Use Committee and were performed in accordance with the guidelines of the institution. *Npc1*$^{-}$ mice were obtained by heterozygous mating.

KN-93 phosphate (MCE, #HY15465B) was dissolved in DMSO and diluted to 0.2 mg/ml in phosphate-buffered saline (PBS) with 10% DMSO. A pair of 7-week-old mice received intraperitoneal injection with KN-93 (5 mg/kg/qod) for 3 weeks. For miglustat treatment, two 7-week-old *Npc1*$^{-}$ mice were fed with 600 mg/kg of miglustat 5 times a day for 3 weeks, and one *Npc1*$^{-}$ mouse was fed with PBS and was euthanized at 9 weeks of age because of weakness. For NALL treatment, three 3-week-old *Npc1*$^{-}$ mice were fed with 100 mg/kg of NALL 5 times a day for 6 weeks. The treatment schedules were also depicted on Fig. S1.

2.2. Immunohistochemical staining procedure

Wild-type and *Npc1*$^{-}$ mice were euthanized at 9 weeks of age and perfused with PBS containing 4% paraformaldehyde (PFA). Frozen tissues were sliced into 25 μm sections. Immunohistochemistry was performed after antigen retrieval in citrate buffer (10 mM sodium citrate, 0.05% Tween-20, pH 6.0) at 90 °C for 15 min. Sections were permeabilized and incubated with primary antibodies [calbindin (1:1000, Novus, #NBP2-50028), cathepsin D (1:100, MyBiosource.com, #MBS448021), GM2 (1:100, Abcam, #ab23942), LAMP1 (1:500, BD Pharmingen, #553792), Rab7 (1:100, Biobyt, #orb180471), CaMK1D (1:150, Novus biologicals, #NBP1-32831), or Flot2 (1:266, Abcam #Ab113661)] diluted in blocking buffer at 4 °C overnight, washed, and then incubated with fluorescence-labeled secondary antibodies (donkey anti-goat, donkey anti-rabbit, goat anti-chick, or goat anti-rat, all at 1:200 dilution). Nuclei were stained with 0.1 μg/ml DAPI in PBS at room temperature for 5 min. For filipin staining, sections were treated in PBS containing 100 mM glycine at room temperature for 10 min and incubated in the dark with 50 μg/ml filipin III (Sigma-Aldrich, #F4767) at room temperature for 45 min. Sections with filipin staining were examined with a Nikon Eclipse TS2 fluorescence microscope. Confocal microscopy images were acquired by Zeiss LSM 510 and analyzed by ZEN software (Carl Zeiss, Jena, Germany) or Leica TCS SP8X and analyzed by LAS X software (Leica Microsystems CMS GmbH, Mannheim, Germany). All experiments were repeated to confirm the results.

2.3. Western blot and analysis of detergent-resistant membranes

Primary antibodies used for Western blot analysis included CaMK1D (1:1000), Rab5a (1:1000, St John's Laboratory, #STJ140061), Tubulin (1:5000, Abcam, #ab7291), Flot2 (1:100, Santa Cruz Biotechnology, #sc-28320), Caveolin 1 (1:1000, Abcam, #ab211503), Clathrin (1:1000, Abcam, #ab129326). For detergent-resistant membranes analysis, mice cerebellar cortex and the DCN were harvested from 9-week-old wild-type or *Npc1*$^{-}$ mice and homogenized in 1 ml lysis buffer (10 mM Tris-HCl pH 7.4, 1 mM EDTA, 1 mM EGTA, 1% Triton X-100, 1 mM Na_3VO_4, 1 mM PMSF and 1X protease inhibitor cocktail) with a dounce homogenizer. 1 ml of 80% sucrose was added to the tissue lysate to a final concentration of 40% sucrose in an ultracentrifugation tube (Beckman coulter 331372),

and overlaid with 4 ml 30% sucrose and 4 ml 5% sucrose. After centrifugation in a Beckman Coulter/Optima XPN-100 Ultracentrifuge with an SW41Ti rotor for 18 h at 4 °C, 14 fractions were collected from top of the gradient for Western blot analysis. All experiments were repeated to confirm the results. Quantitative analysis of Western blot results was performed using ImageJ software.

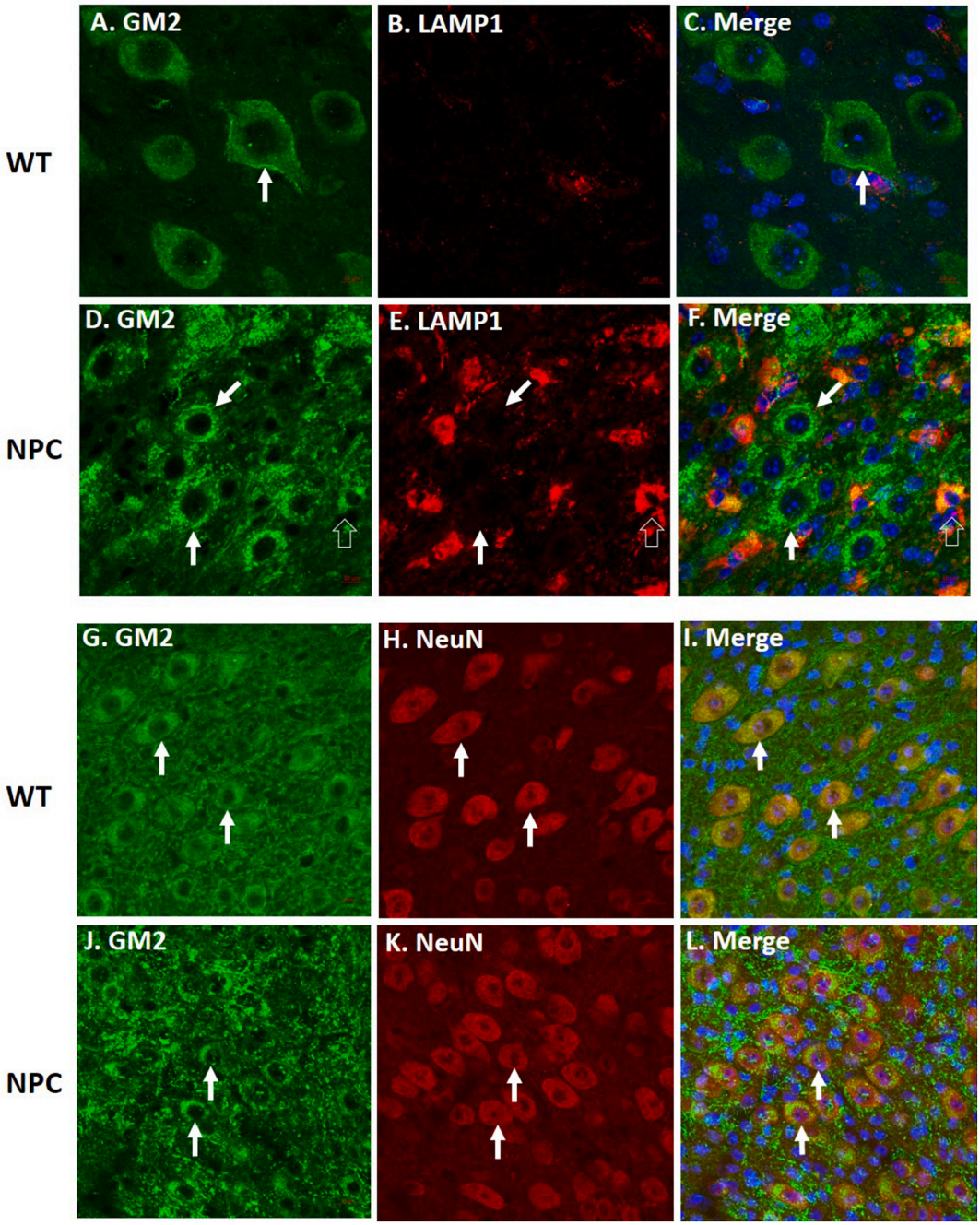

Fig. 1. GM2 accumulation without lysosomal storage in DCN neurons of *Npc1*$^{-}$ mice. (A–C) In wild-type mice, DCN neurons showed moderate GM2 staining (green) but few LAMP1 staining. Focal intense GM2 staining on the cell membrane likely represented lipid rafts (arrows). (D–F) In *Npc1*$^{-}$ mice, DCN neurons showed strong and uneven GM2 staining but were negative for LAMP1 staining (arrows), in contrast to neighboring microglia which showed both LAMP1 and GM2 staining (open arrows). Lipid rafts were never observed in DCN neurons of *Npc1*$^{-}$ mice. (G–I) Double staining for GM2 and NeuN in wild-type mice showed homogenous staining and colocalization. (J–L) Double staining for GM2 and NeuN in *Npc1*$^{-}$ mice showed uneven GM2 staining in cells with homogenous NeuN staining. Cell nuclei were stained with DAPI in the merged pictures. (For interpretation of the references to colour in this figure legend, the reader is referred to the Web version of this article.)

2.4. Single-cell dissociation and single-nucleus RNA sequencing (snRNA-seq)

The cerebellum was first separated from the brains of a pair of 9-week-old wild-type and *Npc1*$^{-}$ mice, and the white matter core region containing the DCN was dissected. The dissected tissue was transferred to 1 ml of lysis buffer (10 mM Tris-HCl, 10 mM NaCl, 3 mM $MgCl_2$, 0.1% Nonidet™ P40, 1 mM DTT, and 50 U/ml RNase inhibitor) and incubated on ice for 15 min. The tissue was then homogenized with a 2-ml Dounce system, washed, and filtered through a 35 μm cell strainer. DAPI was added to the cell suspension at a final concentration of 0.3 μg/ml, and single nuclei were obtained by cell sorting. Approximately 15,000 single nuclei were loaded onto a microfluidic chip with barcoded beads with the Chromium Single Cell 3′ Library & Gel Bead Kit v3, i7 Multiplex Kit, and Chip B

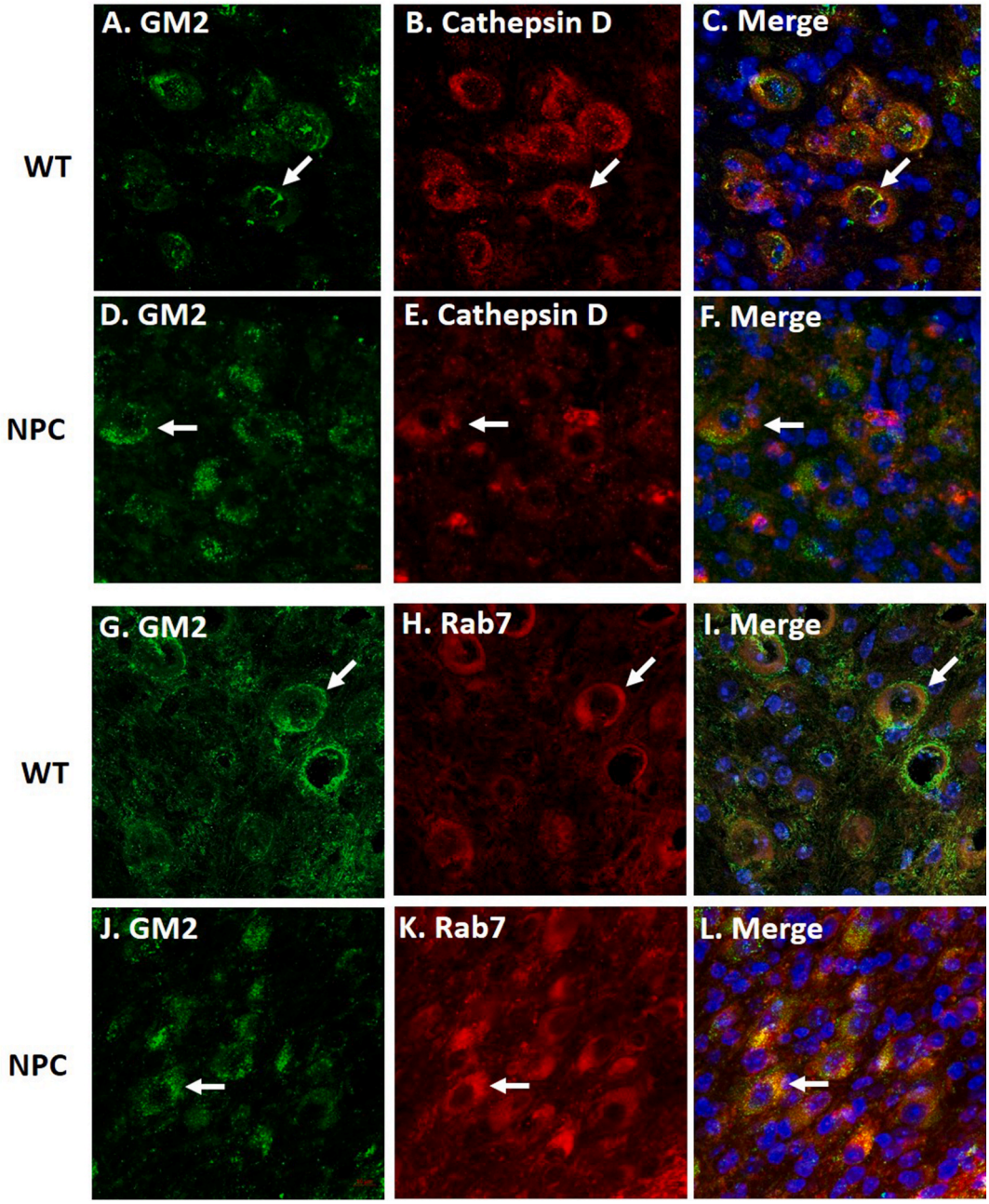

Fig. 2. Cathepsin D and Rab7 staining suggests late-endosomal accumulation of GM2 in DCN neurons of *Npc1*$^{-}$ mice. (A–C) In DCN neurons of wild-type mice, GM2 staining, except for lipid rafts, partially colocalized with cathepsin D staining (arrows). (D–F) In *Npc1*$^{-}$ mice, GM2 and cathepsin D staining did not colocalize inside DCN neurons (arrows). (G–I) In DCN neurons of wild-type mice, GM2 staining did not colocalize with Rab7 staining (arrows). (J–M) In *Npc1*$^{-}$ mice, both GM2 and Rab7 staining was strong and uneven, but colocalized inside DCN neurons (arrow). Cell nuclei were stained with DAPI in the merged pictures.

Kit (10x Genomics). Raw sequencing data from each mouse were quantified using CellRanger 6.0.1 (10x Genomics) with reference transcriptome refdata-gex-mm10-2020-A-R26 based on GENCODE vM23/Ensembl 98 to allow quantification of gene expression. Subsequent analyses were performed using "Seurat v4.0.2" [22]. After filtering, UMI counts were log scale normalized, and the most variable 2,000 genes were used for principal component analysis (PCA), downstream clustering, and t-distributed stochastic neighbor embedding (t-SNE) analysis [23]. Clusters were labeled with cell types based on marker gene expression. Novel clusters were selected and *Rbfox3*-positive cells were rescaled and reclustered to better reveal cellular heterogeneity. Marker genes for each *Rbfox3*+ cell cluster versus all cells of the respective subset were computed using the FindAllMarkers function. A heatmap that shows gene scores for the marker genes in each expression module identified by clustering was plotted by the DoHeatmap function. For Gene Ontology (GO) analysis, the GO term "biological process" was used. The libraries of snRNA-seq were resequenced to confirm the results, but we didn't use the confirmatory dataset.

2.5. Statistical analysis

The Student's *t*-test was employed to compare the Western blot signals and NALL treatment results. Statistics for single-cell studies used built-in functions of individual analytical programs. A p value < 0.05 was considered statistically significant.

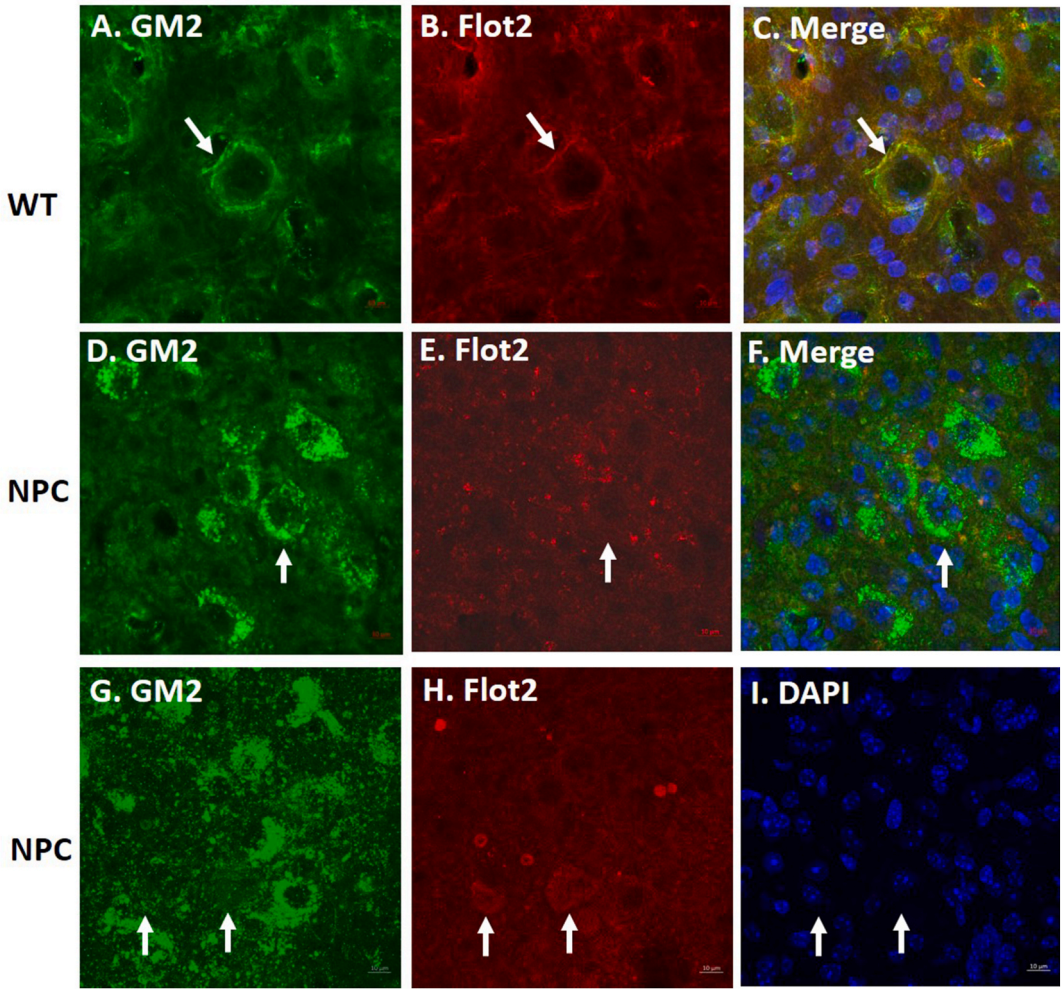

Fig. 3. Flot2 staining decreased in *Npc1*$^{-}$ mice. (A–C) In DCN neurons of wild-type mice, GM2 staining colocalized with Flot2 staining (arrows). (D–F) In *Npc1*$^{-}$ mice, Flot2 staining was decreased in DCN neurons which showed GM2 accumulation (arrows). (G–I) In *Npc1*$^{-}$ mice, occasionally Flot2 staining could be seen in GM2-negative cells.

3. Results

3.1. Loss of Flot2 expression in DCN neurons of Npc1⁻ mice

In the cerebellar cortex of *Npc1*⁻ mice, Purkinje cells was severely decreased in number (Fig. S2), and microglia showed prominent accumulation of LAMP1 and GM2 (Fig. S3). However, in the DCN, most GM2-positive cells were LAMP1 negative (Fig. S4). At high magnification, DCN neurons of wild-type mice revealed homogeneous GM2 staining plus focal intense GM2 membranous staining representing lipid rafts (Fig. 1, A-C, arrows). In *Npc1*⁻ mice, DCN neurons showed strong and uneven GM2 staining but lipid rafts were not found (Fig. 1, D-F, arrows). Moreover, these neurons were negative for LAMP1 staining, in contrast to nearby microglia that were positive for both GM2 and LAMP1 (Fig. 1, D-F, arrowheads). These GM2-positives were also NeuN positive in both wild-type and *Npc1*⁻ mice (Fig. 1, G-L, arrows).

Because of GM2 accumulation was not located in the lysosomes of DCN neurons in *Npc1*⁻ mice, we further performed staining for cathepsin D, a peptidase synthesized in the Golgi apparatus and transported to lysosomes, and for Rab7, a late-endosome marker. In DCN neurons of wild-type mice, GM2 staining, except for lipid rafts, partially colocalized with cathepsin D staining (Fig. 2A–C), while in *Npc1*⁻ mice, GM2 and cathepsin D staining did not colocalize inside DCN neurons (Fig. 2D–F). In DCN neurons of wild-type mice, GM2 staining did not colocalized with Rab7 staining (Fig. 2G–I), while in *Npc1*⁻ mice, both GM2 and Rab7 staining was strong and uneven, but colocalized inside DCN neurons (Fig. 2J-L).

We then performed staining for a lipid raft-specific protein maker, Flot2. The results revealed that Flot2 was colocalized with GM2 in wild-type mice (Fig. 3A–C), however, Flot2 staining was lost in *Npc*1⁻ mice even though GM2 staining was strong. (Fig. 3D–F). In the DCN of *Npc*1⁻ mice, occasionally Flot2 staining could be seen in GM2-negative cells (Fig. 3G–I). We further performed Western blot analysis for cerebellar cortex and DCN tissues from wild-type and *Npc1*⁻ mice (Fig. S5). The proteins we analyzed included plasma membrane associated proteins Flot2, Caveolin 1, and Clathrin, and cytoplasmic proteins Rab5a and CaMK1D. However, there was no significant change in DCN to cortex ratio of these proteins in *Npc1*⁻ mice. We observed variability of caveolin 1 expression in the cerebellar cortex of *Npc1*⁻ mice, but we did not know its etiology. We further analyzed detergent resistant membranes, which represents lipid rafts, for cerebellar tissues by sucrose density fractionation. The results showed the presence of lipid rafts in fractions 6 and 7 in both cerebellar cortex and DCN tissues of wild-type and *Npc1*⁻ mice (Fig. S6). We concluded that these assays were not suitable for our purpose, because we were interested in a small fraction of cells in the tissues included in the assays.

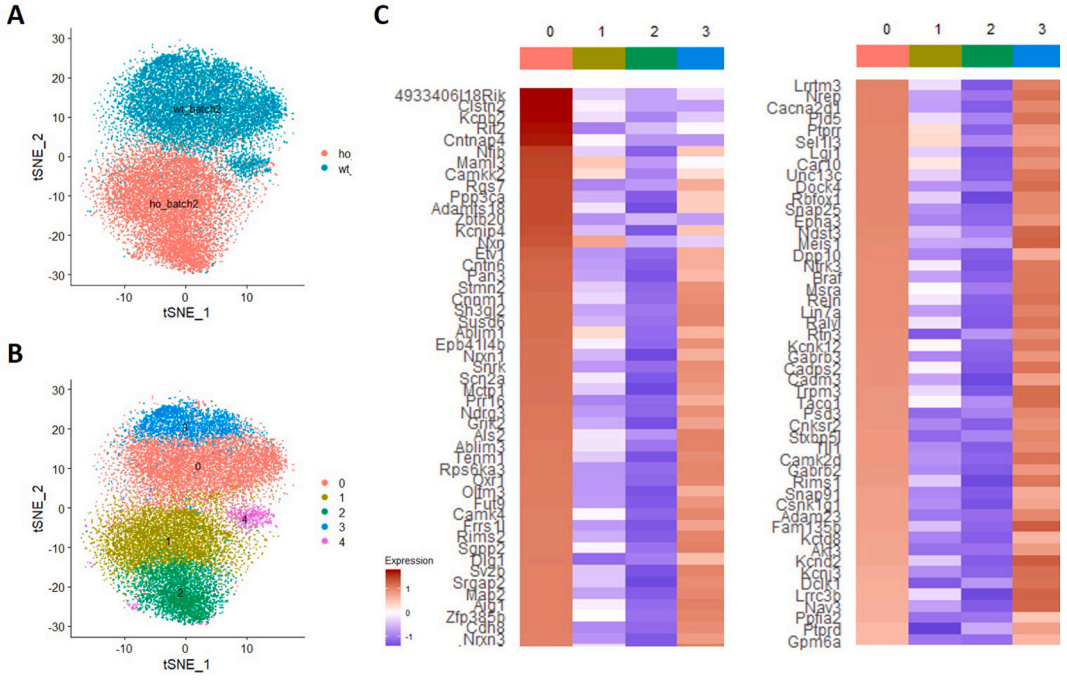

Fig. 4. Reduced gene expression in DCN neurons of *Npc1*⁻ mice. (A) Two-dimensional t-SNE distribution analysis of snRNA-seq data showed distribution of *Rbfox3*-expression cells from wild-type and *Npc1*⁻ mice. (B) Five cell clusters contained DCN neurons. Cells in clusters 0, 3, and 4 were from wild-type mice, and cells in clusters 1 and 2 were from *Npc1*⁻ mice. (C) A heatmap ranked by gene expression level in cells from cluster 0. Cells from clusters 1 and 2 showed a lower gene expression level in comparison to cells from clusters 0 and 3.

3.2. snRNA-seq revealed a generalized reduction in gene expression in DCN neurons of *Npc1*$^{-}$ mice

To explore the disturbances occurred in DCN neurons of *Npc1*$^{-}$ mice, we performed snRNA-seq for a pair of 9-week-old mice, and more than 50,000 reads per cell were obtained. There was a mean of 1,050 genes identified per cell in wild-type mice [24], but there was only a mean of 456 genes per cell in *Npc1*$^{-}$ mice. Two-dimensional t-SNE distribution of merged data from the two mice discriminated clusters of microglia, oligodendrocytes, oligodendrocyte precursor cells, etc. (Fig. S7). The rest of *Rbfox3*-expressing cells were defined as DCN neurons. DCN neurons were further separated into five clusters: cells in clusters 0, 3, and 4 were from the wild-type mice, and cells in clusters 1 and 2 were from the *Npc1*$^{-}$ mice (Fig. 4A and B). When we drew a heatmap ranked by gene expression level of cluster 0, the largest cluster in wild-type mice, we observed a generalized decrease in gene expression in clusters 1 and 2 which were from *Npc1*$^{-}$ mice, but not in cluster 3 which was from wild-type mice (Fig. 4C). We then performed GO analysis for the top 20 expressed genes in these clusters (except for cluster 4 which contained few cells). The results revealed that in wild-type mice, synaptic genes were enriched in clusters 0 and 4, and channel/transporter genes were enriched in cluster 3 (Fig. S8). However, there was a lack of features in *Npc1*$^{-}$ mice clusters 1 and there was no feature in cluster 2.

3.3. CaMK inhibitor exaggerates *Camk1d* overexpression in *Npc1*$^{-}$ mice

Although the gene expression level in *Npc1*$^{-}$ mice was generally low, the expression of *Camk1d*, the most abundant Ca^{2+}/calmodulin-dependent protein kinase (CaMK) gene expressed in mouse DCN neurons, was higher than in wild-type mice ($p < 0.001$) (Fig. S9). We first confirmed the submembranous accumulation of CaMK1D in DNC neurons of *Npc1*$^{-}$ mice by immunohistochemistry (Fig. 5A–H). We wondered if CaMK inhibitor KN-93 could be a treatment for NPC. We then injected 7-week-old mice with KN-93 for three weeks, but found that CaMK1D staining became even stronger in both wild-type and *Npc1*$^{-}$ mice (Fig. 5I-L). It is possible that the increase in *Camk1d* expression in *Npc1*$^{-}$ mice was because of a deficiency of CaMK1D activity, and the inhibitor treatment just worsened the situation.

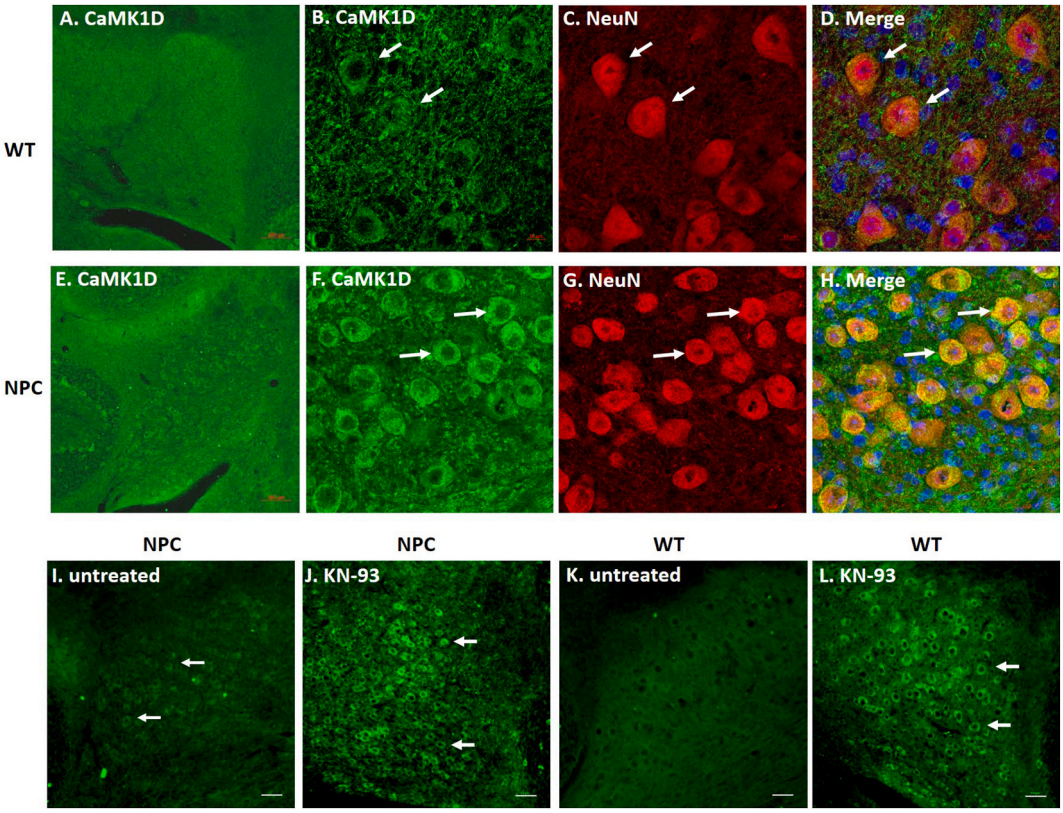

Fig. 5. The elevation of CaMK1D expression in DCN neurons of *Npc1*$^{-}$ mice was aggravated by a CaMK inhibitor. (A–D) In wild-type mice, CaMK1D staining could be seen in NeuN-positive DCN neurons (arrows). A low-magnification picture was showed in panel A. (E–H) In *Npc1*$^{-}$ mice, CaMK1D accumulated in the submembranous space of DCN neurons (arrows). A strong contrast between CaMK1D-stained neurons and the background staining was observed in a low-magnification picture in panel E. (I–J) KN-93 treatment further increased CaMK1D staining in DCN neurons of *Npc1*$^{-}$ mice (arrows). (K–L) KN-93 treatment also increased CaMK1D staining in wild-type mice (arrows).

3.4. Miglustat treatment increased Flot2 expression in Npc1⁻ mice

Miglustat is an approved drug for NPC. Miglustat decreases the synthesis of sphingolipid and relieves the symptoms of patients with NPC [12,13]. We fed two 7-week-old *Npc1*⁻ mice with miglustat for 3 weeks. All two miglustat-treated mice survived to the 10-week endpoint, while one PBS-treated mouse only survived to 9 weeks. Miglustat-treated *Npc1*⁻ mice did not show a significant decrease in GM2 staining, but faint Flot2 staining could be seen in NeuN-positive DCN neurons (Fig. 6I–L). A few NeuN-negative cells also showed Flot2 staining (Fig. 6I-L, arrowheads).

3.5. NALL treatment recovered Flot2 expression in Npc1⁻ mice

N-acetyl L-leucine (NALL) is a drug under investigation for the treatment of NPC. The mechanism of NALL is still not clear, but the drug has been shown to decrease the symptoms of treated mice and patients with NPC [16]. We fed three 3-week-old *Npc1*⁻ mice with NALL for 6 weeks. The treated mice revealed less tremor at 6 months of age, and a slightly better body weight at 8 months of age ($p = 0.244$). DCN neurons of treated *Npc1*⁻ mice did not show a significant decrease in GM2 accumulation, but Flot2 staining was recovered (Fig. 6M–P). In the cerebellar cortex, recovery of GM2 and Flot2 expression also occurred in molecular layer neurons (Fig. S10).

4. Discussion

NPC is commonly classified as a lysosomal storage disease, but late endosomal sphingolipid and cholesterol accumulation is also observed in cultured skin fibroblasts [7,10] and neurons in the brain (the current study). Possible etiologies for late endosomal storage

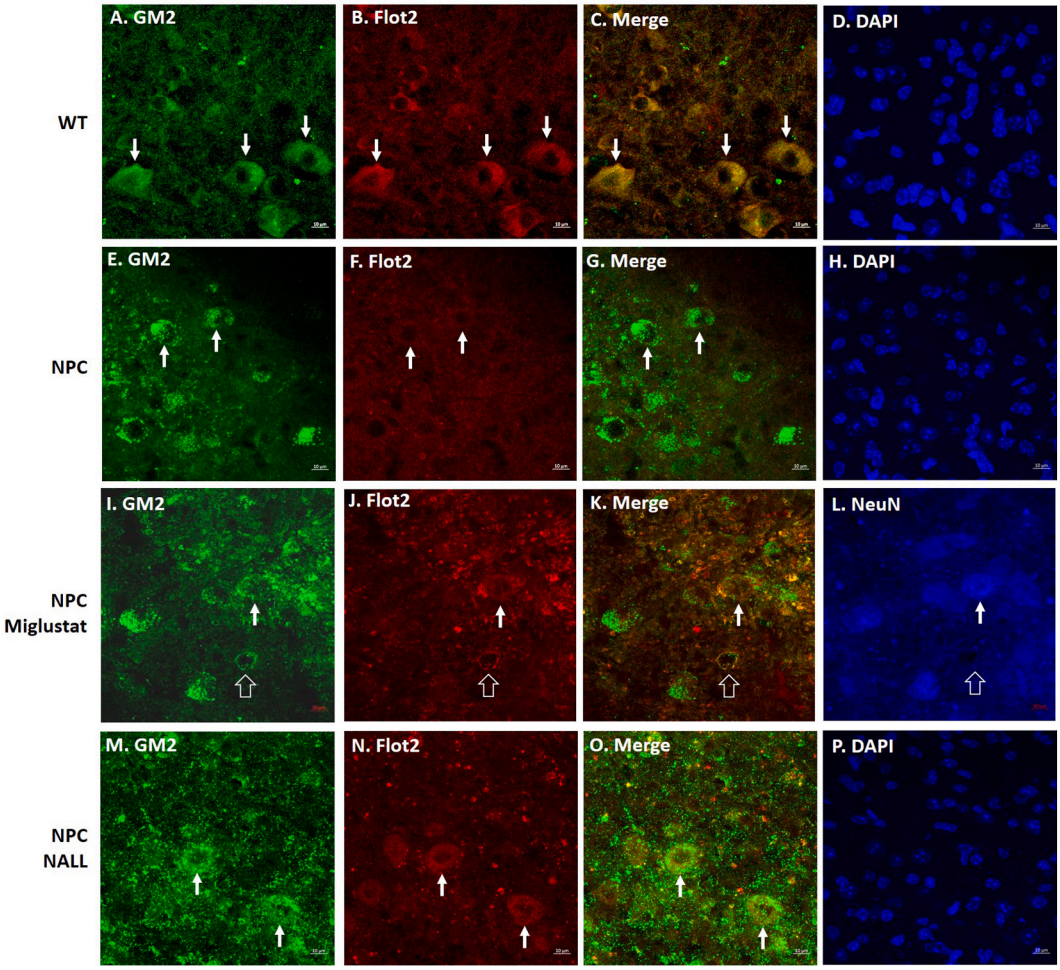

Fig. 6. Systemic treatments rescued the expression of Flot2 in DCN neurons of *Npc1*⁻ mice. (A–D) GM2 and Flot2 double staining for DCN neurons of wild-type mice. (E–H) In *Npc1*⁻ mice, no Flot2 staining was found in DCN neurons which showed strong GM2 staining (arrows). (I–L) In the miglustat-treated *Npc1*⁻ mice, faint Flot2 staining could be seen in NeuN-positive DCN neurons (arrows). A few NeuN-negative cells also showed Flot2 staining (arrowheads). (M – P) In the N-acetyl L-leucine (NALL)-treated *Npc1*⁻ mice, Flot2 staining was like that in wild-type mice (arrows).

in NPC include cholesterol inhibition of sphingolipid activator proteins [9] or altered calcium homeostasis [10], but altered vesicular transport [8] is more likely the etiology in the brain where there is no increase in unesterified cholesterol. Cells normally internalize proteins and lipids in the plasma membrane by endocytosis, and recycling from early endosomes returns the endocytosed proteins and lipids back to the plasma membrane (Fig. 7A) [25]. Upon the deficiency of NPC1, membrane-derived sphingolipids, including GM2, are diverted to and sequestrated in the late endosomes [8] and can't be recycled back to the plasma membrane. We hypothesize that the loss of Flot2 could be caused by the deficiency of sphingolipids in the early endosome and plasma membrane (Fig. 7B). Flot2 loss occurred in neurons with GM2 accumulation, and Flot2 staining could be seen in GM2-negative cells in the DCN of *Npc1*$^{-}$ mice.

Lipid rafts are dynamic, sterol- and sphingolipid-enriched domains that segregate specific elements to regulate their interactions with other membrane components and hence their activity [21]. Flot2 is a lipid raft scaffold protein. Flot2, after phosphorylation by Fyn, a Src kinase, triggers raft-dependent endocytosis [26]. Flot2 is involved in cell polarization as well as actin cytoskeletal organization, and has been associated with different malignancies [27]. Precious data also suggest that the loss of Flot2 plays a key role in the pathogenesis of NPC. In skin fibroblasts derived from patients with NPC, interruption of NPC1-dependent recycling of cholesterol was observed [28], and the formation of NPC1-Flot2-cholesterol membrane microdomains was also demonstrated [29]. In one recent study, fibroblasts isolated from NPC patients showed shift in Flot2 distribution, although treatment with Miglustat did not normalize this defect [30].

The functional disturbances we observed in DCN neurons, low gene expression and dysregulation of CaMK1D, could both be attributed to the loss of lipid rafts. Normally DCN neurons receive inhibitory signals from Purkinje cells, and upon the loss of Purkinje cells, DCN neuron activities should increase. However, our snRNA-seq study revealed a generalized decrease in gene expression in DCN neurons, suggesting abnormalities in plasma membrane signaling. The dysregulation of CaMK1D could also be the consequences of plasma membrane dysfunction. CaMKs are a group of membrane receptor-associated protein kinases [31], and we demonstrated that CaMK1D was the major type of CaMKs expressed in DCN neurons (Fig. S9). CaMK1D is likely associated with membranous GABAergic receptors that receive signals from Purkinje cells. In the current study, CaMK inhibitor induced a rise in CaMK1D expression in both wild-type and *Npc1*$^{-}$ mice. This compensatory process suggested that CaMK1D activity in DCN neurons was already deficient, probably due to the loss of lipid rafts.

If the loss of Flot2 expression is a key component in the pathogenesis of NPC, current treatments effective in NPC patients should correct this defect. Miglustat decreases the synthesis of sphingolipids and has been approved to treat NPC [13]. We demonstrated that a

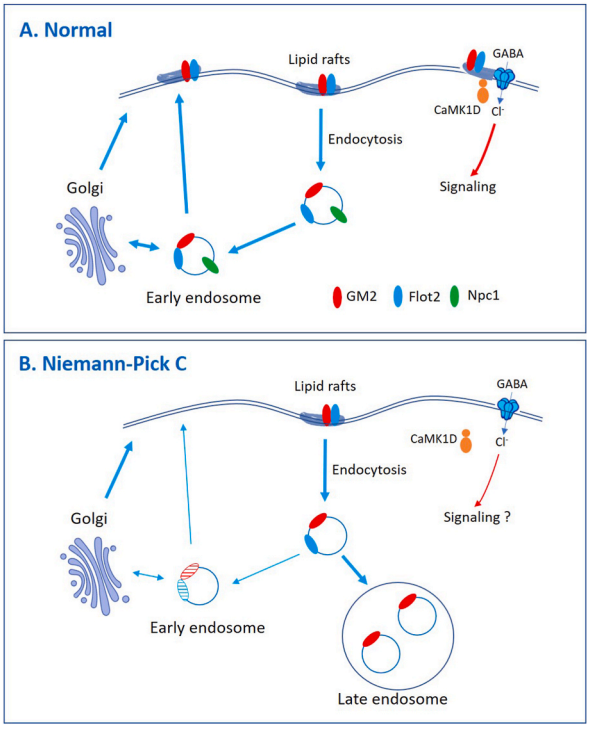

Fig. 7. Proposed mechanism of cerebellar neuron dysfunction in NPC. (A) In normal neurons, lipid rafts, containing both gangliosides (represented by GM2) and Flot2, play an important role in cell function. For example, both GABA receptors, which accept Purkinje cell signaling, and CaMK1D, which modifies membranous receptor signal transduction, are associated with lipid rafts. Plasma membranous lipids and proteins can be internalized by endocytosis, and recycled back through early endosomes and NPC1 is necessary for these processes. (B) In cerebellar neurons from *Npc1*$^{-}$ mice, there is no NPC1 expression. The endocytosis vesicles are diverted to late endosomal multivesicular bodies, where GM2 accumulated but Flot2 was degraded. The plasma membrane is deficient of GM2 and Flot2, and lipid rafts cannot be organized. Membrane receptors and submembranous proteins cannot be associated lipid rafts and signaling is deranged.

3-weeks treatment with miglustat increased the expression of Flot2 (Fig. 5). NALL, a modified amino acid, has been used to treat neurodegenerative diseases including NPC, GM2 gangliosidoses, and ataxia telangiectasia [32], even though the mechanism of this drug is still not clear. Surprisingly, a 6-week treatment with NALL effectively recovered Flot2 expression in neurons (Figs. 5 and 6). Therefore, restoration of lipid rafts is likely the mechanism for NALL to improve ataxia in patients with NPC.

There are two major limitations of the current study. First, we studied small groups of neurons in the cerebellum. Bulk quantitative assays like the Western blot and detergent-resistant membranes assay may not show abnormalities in a small portion of cells in the specimen. Second, maintenance and treatment of *Npc1*$^{-}$ mice were difficult because of the high mortality of the animals, and therefore the number of experimental animals in the current study was small. We were not able to overcome these limitations, because isolation of intact neurons from mouse brain is a difficult job and even whole DCN offered barely enough material for Western blot and detergent resistant membranes analyses. However, our morphologic IHC studies showed clear results and have all been repeated. Therefore, our cell function change data were reliable, and for the drug treatment studies, drug effects were evident in the studies, even though survivals couldn't be assessed because of the small in number.

5. Conclusion

Through the study of DCN neurons, we found that disruption of lipid rafts, represented by loss of Flot2 expression, was a key pathological process in NPC. The efficacy studies of current treatments for NPC on Flot2 expression not only enforce our hypothesis for the pathogenesis of NPC, but also open a new hope to improve the treatment for NPC.

Author contribution statement

Tsu-I Chen, Pei-Chun Hsu: Conceived and designed the experiments; Performed the experiments; Analyzed and interpreted the data.

Ni-Chung Lee, Yin-Hsiu Chien: Analyzed and interpreted the data.

Yu-Han Liu, Hao-Chun Wang, Yen-Hsu Lu: Performed the experiments.

Wuh-Liang Hwu: Conceived and designed the experiments; Wrote the paper.

Data availability statement

Data will be made available on request.

Funding and additional information

This study was funded by MOST 109-2314-B-002 -133 -MY3.

Declaration of competing interest

The authors declare that they have no known competing financial interests or personal relationships that could have appeared to influence the work reported in this paper.

Acknowledgments

We thank the animal facility at the College of Medicine, National Taiwan University, for caring for the animals.

Appendix A. Supplementary data

Supplementary data to this article can be found online at https://doi.org/10.1016/j.heliyon.2023.e18082.

References

[1] E.D. Carstea, et al., Niemann-Pick C1 disease gene: homology to mediators of cholesterol homeostasis, Science 277 (1997) 228–231.
[2] S. Naureckiene, et al., Identification of HE1 as the second gene of Niemann-Pick C disease, Science 290 (2000) 2298–2301.
[3] M.T. Vanier, et al., Genetic heterogeneity in Niemann-Pick C disease: a study using somatic cell hybridization and linkage analysis, Am. J. Hum. Genet. 58 (1996) 118–125.
[4] W.S. Garver, et al., Localization of the murine Niemann-Pick C1 protein to two distinct intracellular compartments, J. Lipid Res. 41 (2000) 673–687.
[5] M.T. Vanier, Niemann-Pick disease type C, Orphanet J. Rare Dis. 5 (2010) 16.
[6] M.T. Vanier, P. Latour, Laboratory diagnosis of Niemann-Pick disease type C: the filipin staining test, Methods Cell Biol. 126 (2015) 357–375.
[7] T. Kobayashi, et al., Late endosomal membranes rich in lysobisphosphatidic acid regulate cholesterol transport, Nat. Cell Biol. 1 (1999) 113–118.
[8] D. te Vruchte, et al., Accumulation of glycosphingolipids in Niemann-Pick C disease disrupts endosomal transport, J. Biol. Chem. 279 (2004) 26167–26175.
[9] S. Anheuser, et al., Membrane lipids regulate ganglioside GM2 catabolism and GM2 activator protein activity, J. Lipid Res. 56 (2015) 1747–1761.

[10] E. Lloyd-Evans, et al., Niemann-Pick disease type C1 is a sphingosine storage disease that causes deregulation of lysosomal calcium, Nat. Med. 14 (2008) 1247–1255.
[11] D.A. Kelly, et al., Niemann-Pick disease type C: diagnosis and outcome in children, with particular reference to liver disease, J. Pediatr. 123 (1993) 242–247.
[12] Y.H. Chien, et al., Long-term efficacy of miglustat in paediatric patients with Niemann-Pick disease type C, J. Inherit. Metab. Dis. 36 (2013) 129–137.
[13] M.C. Patterson, et al., Miglustat for treatment of Niemann-Pick C disease: a randomised controlled study, Lancet Neurol. 6 (2007) 765–772.
[14] D.S. Ory, et al., Intrathecal 2-hydroxypropyl-beta-cyclodextrin decreases neurological disease progression in Niemann-Pick disease, type C1: a non-randomised, open-label, phase 1-2 trial, Lancet 390 (2017) 1758–1768.
[15] T. Bremova-Ertl, et al., Efficacy and safety of N-acetyl-L-leucine in Niemann-Pick disease type C, J. Neurol. 269 (2022) 1651–1662.
[16] E. Kaya, et al., Acetyl-leucine slows disease progression in lysosomal storage disorders, Brain Commun. 3 (2021) fcaa148.
[17] S.K. Loftus, et al., Murine model of Niemann-Pick C disease: mutation in a cholesterol homeostasis gene, Science 277 (1997) 232–235.
[18] J.R. Sarna, et al., Patterned Purkinje cell degeneration in mouse models of Niemann-Pick type C disease, J. Comp. Neurol. 456 (2003) 279–291.
[19] T. Kodachi, et al., Severe demyelination in a patient with a late infantile form of Niemann-Pick disease type C, Neuropathology 37 (2017) 426–430.
[20] M.Y. Uusisaari, T. Knopfel, Diversity of neuronal elements and circuitry in the cerebellar nuclei, Cerebellum 11 (2012) 420–421.
[21] E. Sezgin, et al., The mystery of membrane organization: composition, regulation and roles of lipid rafts, Nat. Rev. Mol. Cell Biol. 18 (2017) 361–374.
[22] Y. Hao, et al., Integrated analysis of multimodal single-cell data, Cell 184 (2021) 3573–3587 e29.
[23] B. Zhou, W. Jin, Visualization of single cell RNA-seq data using t-SNE in R, Methods Mol. Biol. 2117 (2020) 159–167.
[24] A. Jariani, et al., A new protocol for single-cell RNA-seq reveals stochastic gene expression during lag phase in budding yeast, Elife 9 (2020).
[25] T. Taguchi, Emerging roles of recycling endosomes, J. Biochem. 153 (2013) 505–510.
[26] K. Hanafusa, N. Hayashi, The Flot2 component of the lipid raft changes localization during neural differentiation of P19C6 cells, BMC Mol. Cell Biol. 20 (2019) 38.
[27] R. Kumar, et al., The differential role of the lipid raft-associated protein flotillin 2 for progression of myeloid leukemia, Blood Adv. 6 (2022) 3611–3624.
[28] S. Lusa, et al., Depletion of rafts in late endocytic membranes is controlled by NPC1-dependent recycling of cholesterol to the plasma membrane, J. Cell Sci. 114 (2001) 1893–1900.
[29] J.H. Zhang, et al., The N-terminal domain of NPC1L1 protein binds cholesterol and plays essential roles in cholesterol uptake, J. Biol. Chem. 286 (2011) 25088–25097.
[30] G. Brogden, et al., Different trafficking phenotypes of Niemann-pick C1 gene mutations correlate with various alterations in lipid storage, membrane composition and miglustat amenability, Int. J. Mol. Sci. 21 (2020).
[31] K.U. Bayer, H. Schulman, CaM kinase: still inspiring at 40, Neuron 103 (2019) 380–394.
[32] T. Fields, et al., A master protocol to investigate a novel therapy acetyl-L-leucine for three ultra-rare neurodegenerative diseases: Niemann-Pick type C, the GM2 gangliosidoses, and ataxia telangiectasia, Trials 22 (2021) 84.